

Experimental evidence for reversible zippering of chains in magnetic nanofluids under external magnetic fields

Junaid M. Laskar, John Philip,^{*} and Baldev Raj

Metallurgy and Materials Group, Indira Gandhi Centre for Atomic Research, Kalpakkam 603 102, Tamilnadu, India

(Received 10 June 2009; revised manuscript received 24 August 2009; published 16 October 2009)

We study the time-dependent transmitted intensity and the scattered pattern from magnetic nanofluids at constant ramping of uniform external magnetic field. The nanofluid used is the dispersion of magnetite particles with an average diameter of 6.5 nm with a protective surfactant coating. We observe several critical fields at which the transmitted light intensity decreases drastically followed by the formation of a ringlike pattern on a screen placed perpendicular to the field direction. Interestingly, the critical fields occur at a regular interval of 20 G. The observed critical fields are attributed to zippering transitions of the chains due to attractive energy well when the chains are of different lengths or shifted with respect to one another. Interaction energy calculations show a decrease in the energy of the system due to dipolar interactions at different critical fields confirming the lowering of the system energy through lateral coalescence. The observed zippering phenomenon is perfectly reversible.

DOI: [10.1103/PhysRevE.80.041401](https://doi.org/10.1103/PhysRevE.80.041401)

PACS number(s): 83.80.Hj, 83.80.Gv, 64.70.Nd, 89.75.Fb

I. INTRODUCTION

The interesting physical properties of colloids make them a model system for fundamental studies to a wide range of potential applications [1–3]. Localization of light in disordered media has been a topic of intense research during the last few decades [4–6]. Magnetic colloids can be easily manipulated with an external magnetic field, and hence they are exciting system both from fundamental and application points of view [7–11]. Complete understanding of the structure, phase behavior, and dynamics of strongly interacting dipolar magnetic fluids is still a considerable challenge to soft matter physics. The richness of structures including chains, columns, and labyrinthine patterns that can be formed in dipolar magnetic fluid system makes them very interesting [12–17]. The full phase diagram unfolding the colloidal crystal structures in the presence of external field spanning from zero to high field limit is presented for both the cases of dipolar hard and soft spheres [18]. The field-induced aggregation kinetics of magnetic colloidal particles has been studied by scattering dichroism [19], Raman spectroscopy [20], optical microscopy with digital image analysis [21,22], light scattering with electron microscopy [23], time-resolved small-angle neutron scattering [24], Monte Carlo modeling [25], molecular and stochastic dynamics simulation [26,27], Brownian dynamics [28], simulation based on a developed computer model [29], and time-dependent light scattering [30].

There have been several interesting studies to understand the behavior of ferrofluids under external magnetic fields [31–36]. Light-induced reversible cluster formation of nanoparticles in magnetic fluids and the dependence of switching speed of magnetic fluids on the incident laser power density have been reported [35,37]. In the presence of external field, the magnetic colloids experience an attractive force along the field direction and repulsive normal to it. Therefore, on

slowly increasing the magnetic field from zero to high value, the magnetic fluid undergoes several interesting structural transitions [12,32]. At first, the randomly oriented dispersed Brownian particles undergo head-to-tail aggregation forming chains aligned along the field direction. Due to the lateral coalescence of the chains, they form columns by undergoing secondary aggregation [14,16]. Thermal-fluctuation-induced interactions and perturbations in the local lateral field due to topological defects in the dipolar chains are attributed for their lateral coalescence [38,39]. The form of interaction energy between two chains of magnetorheological colloids as a function of distance is always attractive in nature for head-to-tail aggregation, whereas for lateral aggregation it has repulsive component as well [40]. This means that there is significant energy barriers associated with the lateral aggregation of dipolar chains. These energy barriers prevent the magnetic colloids from reaching the lowest-energy state consisting of thicker columns of clustered chains. Using analytical and numerical analysis it has been speculated that column sizes seen in the experiments are not representative of the equilibrium structure [41]. True experimental results that describe equilibrium phenomena from metastable state are still unclear.

Due to the lateral aggregation and coalescence of the chains into thicker columns the total scattering cross section for the light transmitting parallel to the field gets decreased that results in the increase in the transmitted light. This was predicted by computer simulations [42] and also confirmed experimentally [42,43]. In this paper, using time-dependent light scattering measurement at constant ramping of external magnetic field values, we investigate metastable structures formed in a magnetically polarizable media. The time-dependent variation in the transmitted intensity and the scattered pattern indicates structural transitions at certain critical magnetic fields. The structures inside the dipolar fluid for different regimes of magnetic field are modeled by considering linear aggregation at the first and lateral aggregations at the next higher critical fields. Based on these modeled structures the reason for the experimentally observed scattered

^{*}Corresponding author; philip@igcar.gov.in

patterns and their variations at the critical fields are explained. The increase in the stability of the system due to the structural reorganization at the critical fields is explained on the basis of energy argument. Our experiments suggest that the lateral aggregations can be observed only if the experiment is performed at very slow ramping rates.

II. EXPERIMENTAL SETUP AND PROCEDURE

The dispersion used in our studies was a magnetic nanofluid where the particle size is less than the incident light wavelength $a < \lambda$. We measure the forward transmitted light intensity as a function of time at different applied magnetic fields. We used a stable colloidal suspension of magnetite (Fe_3O_4) nanoparticles with an average diameter of 6.5 nm, coated with oleic acid and dispersed in a hydrocarbon like octane. The organic layer thickness around the particles is about 1.5 nm. The polydispersity index (PDI) is measured by dynamic light scattering using a Nano ZS apparatus, Malvern Instrument. The PDI accounts for the relative error between curve fit and experimental values. A suspension with a PDI value lower than 0.1 is considered as fairly monodisperse. The polydispersity index of our sample was 0.092. The suspensions used in our experiments had an excellent long-term stability with no agglomerations even after prolonged application of very strong magnetic fields. The ferrofluid sample is taken in a quartz cuvette and kept inside a solenoid, where magnetic field is varied by changing the current passing through its coil using a dc power supply. The direction of magnetic field is parallel to the light propagation. An amplitude and frequency stabilized polarized He-Ne laser (Spectra-physics) with a wavelength of 632.8 nm and with an output power of 1 mW is used as a light source. The light intensity is measured by using a photomultiplier (PMT) tube (Oriel). The output of the PMT is fed to readout through a current amplifier with variable gain. The analog output from the readout is connected to a 12 bit analog-to-digital converter (ADC) that is interfaced with a computer. For observation, the scattered light from the sample is projected on a screen and recorded using a charge coupled device (CCD) camera. The transmitted light intensity through the sample has been acquired as a function of time at different external magnetic field values. The variation in the magnetic field within the sample was less than 1% and the variation within the laser spot diameter was less than 0.01%.

The magnetic field is increased in steps of 6.43 G. After each increment, the intensity is measured for 120 s. If there is no intensity variation within this time, the field is increased to another value. If the intensity varies, then it is measured as a function of time until it reaches a stable value. The pattern of the scattered light is also recorded using a CCD camera.

III. RESULTS AND DISCUSSION

A. Transmitted light intensity at different critical magnetic fields

Figure 1 shows the normalized transmitted intensity as a function of time required for the stabilization of intensity at

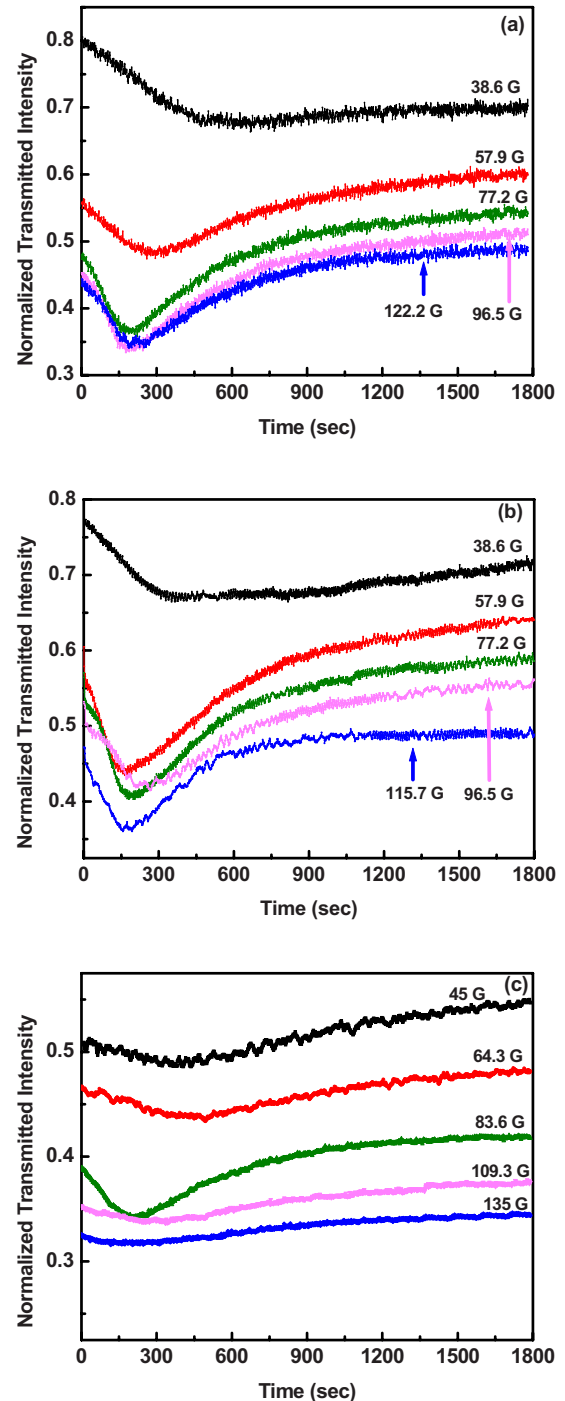


FIG. 1. (Color online) Normalized transmitted intensity as a function of time required at different critical magnetic fields for concentrations of ferrofluid sample (a) 1.078, (b) 0.819, and (c) 0.649 vol %.

different critical magnetic fields for different concentrations. The magnetic field values at which the temporal variation of transmitted intensity is observed are termed as the “critical” fields. The transmitted intensity is normalized with respect to the absolute value of intensity in the absence of any magnetic field. At the critical fields, the intensity starts to decrease with time until it reaches a minimum value. After the minimum, the transmitted intensity again increases until its

value gets saturated at a particular time. For all the concentrations of the sample, five critical fields are observed as the magnetic field is increased up to 200 G. Beyond the above-mentioned value, the field could not be increased further due to overheating of the solenoid coil.

B. Temporal evolution of the scattered pattern at different critical magnetic fields

Figure 2 shows the changes occurring in the scattered pattern and transmitted spot intensity with time at different critical magnetic fields for a dispersion of 0.649 vol %. When the magnetic field value is increased to the first critical field, the scattered pattern contains only a diffused spot as shown in Fig. 2(A). As time progresses, diffused scattered speckles appear around the spot with a decreased spot intensity. With further increase in time, the spot intensity starts to increase after reaching a minimum while the diffused scattered speckles transform into a ringlike structure with the spot on the circumference. As the time elapses further, the ring becomes sharper with increasing spot intensity. The ring becomes sharper when the spot intensity reaches a stable value. Until the field reaches the second critical field, no change in either transmitted spot intensity or in the scattered pattern is observed in the intermediate field values. Although every increment of the field step makes the transmitted spot intensity to decrease a little bit and scattered ring pattern becomes sharper, their time-dependent variations take place only at the critical fields. Figure 2(B) shows the changes occurring in the scattered pattern with time at the second critical magnetic field. As the spot intensity starts to decrease with time at this field, the ring pattern starts to melt. The ring becomes most diffused with maximum scattered light when the spot intensity reaches its minimum. The sharpness of the ring again increases as the spot intensity increases. Finally, both the sharpness of the ring and the spot intensity reach their maximum when the spot intensity gets stabilized after a long time interval. After this, three more critical fields are observed as the field is continued to increase at a constant ramping rate. These fields are named as third, fourth, and fifth critical fields. The time evolution of the scattered pattern at these three critical fields is similar to that of the second one. Again, no variation in the scattered pattern is observed in the intermediate step between the critical fields. When the scattered pattern gets stabilized, the ring becomes sharper after each critical field. The time required for the stabilization of the scattered pattern shows a gradual decrease with increasing critical fields.

Figure 3 shows the evolution of scattered pattern with their corresponding surface plots at the fifth critical magnetic field for 0.649 vol % of the sample. To explain the variations in the transmitted spot intensity and the scattered pattern at the critical fields, it is necessary to know the kind of aggregation and the subsequent structural changes that take place in the dispersion.

In the absence of any external magnetic field, the magnetic nanoparticles are dispersed with their moments oriented in random directions. The magnetite nanoparticles in suspensions acquire dipole moments in the presence of external

magnetic field. The magnitude of the induced dipole moment of an individual nanoparticle is given by

$$m = \frac{\pi}{6} a^3 \chi H_0, \quad (1)$$

where a is the diameter of the nanoparticles, χ is the effective susceptibility of individual nanoparticles, and H_0 is the magnitude of the external magnetic field. The anisotropic interaction energy U_{ij} between two identical parallel point dipoles with magnitude m is given by [40]

$$U_{ij}(r_{ij}, \theta_{ij}) = \frac{m^2 \mu_0}{4\pi} \left(\frac{1 - 3 \cos^2 \theta_{ij}}{r_{ij}^3} \right), \quad (2)$$

where μ_0 is the magnetic permeability of free space, r_{ij} is the magnitude of the vector describing the distance between the centers of i th and j th nanoparticles, and θ_{ij} is the angle between the vector \mathbf{r}_{ij} and the external field vector. The effective magnetic interaction between two magnetic nanoparticles can be described by the coupling constant

$$L = - \frac{U(a, 0)}{k_B T} = \frac{\pi \mu_0 a^3 \chi^2 H_0^2}{72 k_B T}. \quad (3)$$

The coupling constant is the ratio of the maximum magnitude interaction energy to the thermal energy ($k_B T$) in the system. Here, k_B is the Boltzmann constant and T is the temperature. The magnetic nanoparticles in the dispersion self-assemble into aligned structures when $L \gg 1$. As the magnetic field is increased in steps, the moments of the particles start to align themselves along the field direction.

The magnetic field around an infinite chain of magnetic dipoles is given by [16]

$$H(\rho, z) \approx - (2\pi)^2 \left(\frac{m}{4\pi \mu_0 \rho^2 a} \right) \left(\frac{a}{\rho} \right)^{1/2} e^{-2\pi \rho/a} \cos(2\pi z/a), \quad (4)$$

where z is the position along the chain in the applied field direction, m is the particle moment, and μ_0 is the vacuum magnetic permeability. This field decays exponentially with distance ρ in the plane orthogonal to the chain. The integral over the dipole moment density with the field gives the lateral interaction between two chains. According to Hasley-Toor (HT) model, Landau-Peierls fluctuations exhibited by dipolar chains suspended in a three-dimensional (3D) fluid result in long range coupling between them that gives rise to attractive interaction with a power-law decay [44]. The longitudinal and the transverse particle fluctuations of wave vector \mathbf{k} in a dipolar chain create local variations in the concentration of dipoles. This introduces fluctuations in the lateral field. The summation of the interaction energy between the fluctuations of the chains and the energy of deformation required for the fluctuation mode gives the total interaction energy. The interaction has a strong peak at $k\rho \cong 1$ indicating that only fluctuation with wavelength on the order of the separation distance will interact strongly. The total free energy for the chains is

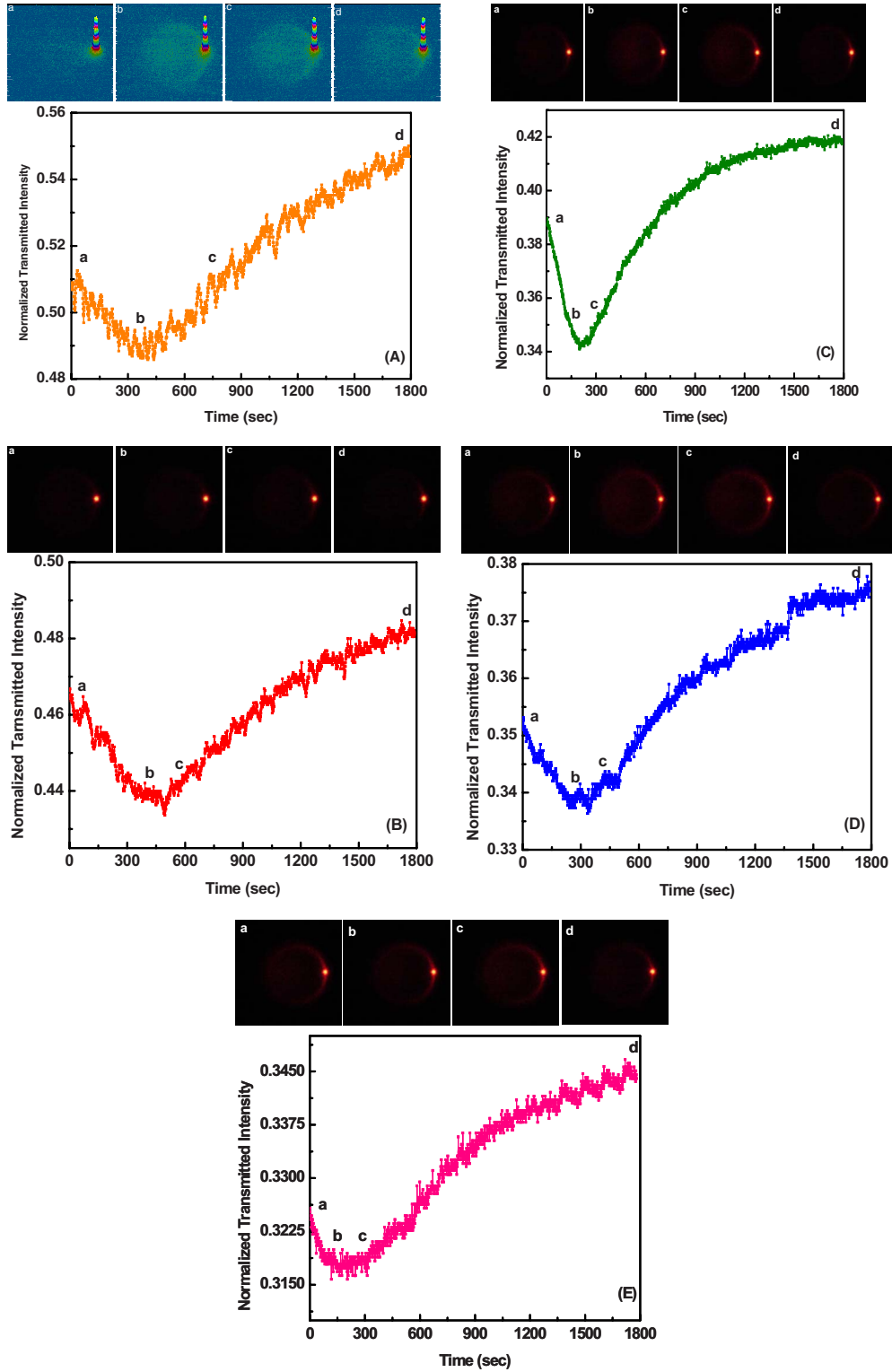


FIG. 2. (Color online) Normalized transmitted spot intensity vs time at (A) first, (B) second, (C) third, (D) fourth, and (E) fifth critical magnetic fields for 0.649 vol % of the sample. On top of each figure, the scattered patterns (surface plot for the first critical field) observed on a screen placed perpendicular to the field direction at different time intervals (marked a–d on the figures) are shown.

$$F(\rho) = -176 \frac{k_B T L a^4}{2\pi \rho^5}. \quad (5)$$

$$\langle H^2 \rangle \sim \frac{m^2 k_B T}{\mu_0^2 \rho^4 a^2 \epsilon} \sim \frac{k_B T a}{\mu_0 \rho^4}. \quad (6)$$

The mean-squared field around the fluctuating chain is given by

From the above equation it is clear that the lateral interaction is independent of the applied field strength and decays as a

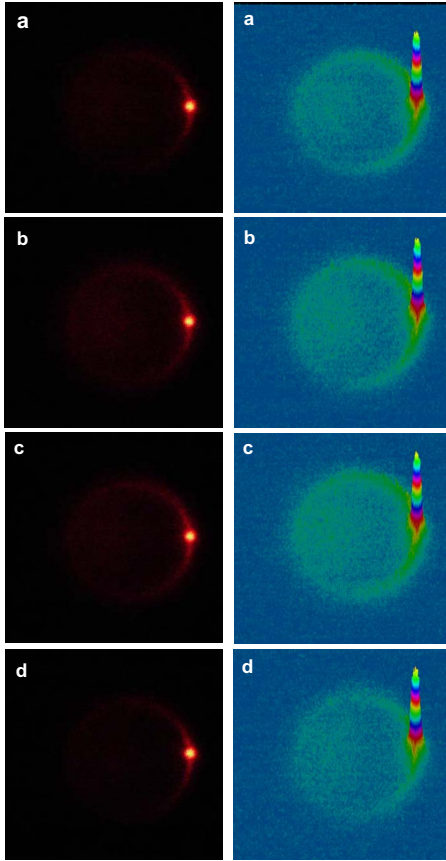


FIG. 3. (Color online) The evolution of scattered pattern with their corresponding surface plots at the fifth critical magnetic field for 0.649 vol % of the sample.

power law. Since in our case the observed changes in the experimental parameter take place at some critical fields only, the possibility of lateral interaction due to the fluctuation of dipolar chains can be ruled out.

To account for the observed dependence of suspension coarsening on field strength, the HT model is modified by Martin and co-workers [39]. The chain with a dipole moment per unit length $m/a \sim \mu_0 \chi a^2 H$ interacts with mean-squared lateral field induced by chain fluctuations. Using Eq. (6) the interaction energy per unit length a is on the order of

$$U \sim (m/a) \langle H^2 \rangle^{1/2} \sim \frac{\chi H (\mu_0 k_B T)^{1/2} a^{5/2}}{\rho^2} \quad (7)$$

and can be either repulsive or attractive. This energy has a strong dependence on the field strength H and separation ρ between the chains. As the field is increased the structural transition of the system takes place at different critical fields. In the field values between the critical fields, the separation ρ remains the same, but the field strength H increases which results in an increase in the interaction energy per unit length U . Two chains laterally coalesce when this energy becomes sufficient enough to overcome the potential-energy barrier for the lateral aggregation. Due to the lateral aggregation at the critical fields the separation distance ρ between the columns now increases which results in a decrease in U . This

decreases the overall energy of the system. Again, at the next higher critical fields the phenomena gets repeated, i.e., the overcoming of the potential barrier for lateral aggregation and the decrease in the total energy of the system after the aggregation due to above-mentioned reasons. These are the plausible reasons for the appearance of critical fields at regular intervals.

Chain defects also create local variations in the dipole moment density along a chain and break the symmetry of the lateral field, which is shown by computer simulation [42]. The defect-driven interaction is predominant (applicable) only at high dipole strengths for moderate and high particle concentrations. Since in our case the system is not exposed to high field, the possibility of the effect of this kind of interaction can be ruled out.

At the first critical field, the particles start self-assembling themselves as doublets, triplets, short chains, and so on which increases the size of scatterers in the system. The increase in length of the chains at a particular magnetic field is a time-dependent process [22]. The reason for the decrease in the transmitted intensity due to the occurrence of resonance in the scattering efficiency resulting from the increase in scatterers' size is discussed in detail recently [45]. No variation either in the transmitted intensity or in the scattered pattern until the first critical field confirms the absence of aggregates. The length of the chains continues to increase with time at the first critical field until they attain the path length of the cell along the field direction. As time progresses, the gap between the chains also opens up with their increase in length. This causes the light transmission to increase again after reaching a minimum.

The reason for the appearance of ringlike structure in the scattered pattern is attributed to the scattering from cylindrical surface of the chains [45,46]. The stabilization of ring structure on the scattered pattern and transmitted intensity confirms the completion of chainlike structures that brings the system to equilibrium. Therefore, the time taken for the stabilization of transmitted intensity is the time required for the system to reach equilibrium at the first critical field.

While the transmitted intensity varies with time at the second critical field, structural rearrangement in the system takes place due to the lateral aggregation of the chains. After the transmitted intensity gets stabilized i.e., after the lateral aggregation of the chains, the system consists of columns of double chains distributed uniformly spanning the entire volume of the cell. This arrangement of uniform distribution of double chain columns in the system is retained until the external field is increased to the third one. Again, at the third critical field, these double chain columns undergo lateral aggregation (zippering) among themselves forming four chain columns. As the system comes to equilibrium by the above-mentioned lateral aggregation of the columns, it consists of equally spaced uniformly distributed four chain columns. Again, there is no change in this distribution of columns in the cell until the next critical field is reached. The lateral aggregation of columns among themselves is again repeated at the fourth critical field forming eight chain columns. Figure 4 shows the schematic of the arrangement of nanoparticles before and after aggregation at different critical magnetic fields. Zero variation in the scattered and transmitted

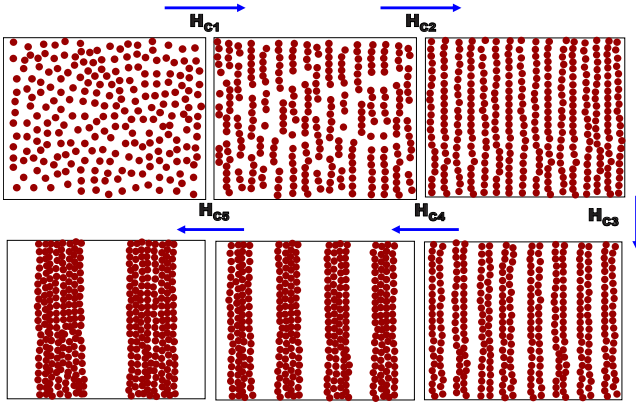


FIG. 4. (Color online) Schematic of the arrangement of magnetic nanoparticles in the dispersion before and after aggregation at different critical fields H_{C1} , H_{C2} , H_{C3} , H_{C4} , and H_{C5} .

intensity confirms the absence of any aggregation process between any two critical fields.

While the chains and columns undergo lateral aggregation at the second and higher critical fields, the fluctuation deviates the scattering surface from the cylindrical one and makes it rough. This fluctuation of the chains and columns also hinders the path of the light transmission. On reaching the equilibrium after the lateral aggregation, the fluctuation is minimized and more space opens up between the columns. This is the reason why the transmitted intensity first decreases and then increases after reaching a minimum. The reason for initial melting and subsequent increase in sharpness of the ring structure in the scattered pattern from the second critical field onward is also the same.

It is important to know whether by undergoing lateral aggregation among the chains or columns from the second critical field onward the potential energy of the system increases or decreases. While calculating the total system potential energy before and after aggregation at different critical fields, the chains and columns shown in Fig. 3 are assumed to be rigid. The total potential energy can be calculated by summing the dipole-dipole interactions [Eq. (2)] between all the particles present in the system. The first step is to calculate the distance between the interacting particles for the given arrangement of columns, cell volume, and number of particles. For this it is required to know the position coordinates of the particles in 3D space corresponding to different arrangements before and after aggregation at the respective critical field. The interparticle spacing (IPS) for a colloidal dispersion of monodisperse spherical particles is given by [47],

$$\text{IPS} = 2r \left[\left(\frac{\phi_m}{\phi} \right)^{1/3} - 1 \right], \quad (8)$$

where r is the radius of particles, ϕ is the particle volume fraction, and ϕ_m is the maximum particle packing fraction (for random dense packing it is 0.63). The volume fraction of a given sample is calculated by using the following formula:

$$\phi = \frac{w_p \rho_f}{(w_p \rho_f) + \rho_p (1 - w_p)}, \quad (9)$$

where w_p is the weight fraction of particles, ρ_p is the density of particles (for Fe_3O_4 it is 5100 kg/m^3), and ρ_f is the density of carrier liquid (for kerosene it is 800 kg/m^3). Now, for a given number of particles in the dispersion, they are arranged in such a way that the maximum number of nearest neighbors are located at the same distance equaling the IPS. This is satisfied when the hexagonal arrangement of particles is considered. The minimum volume required for the above-mentioned arrangement is considered to be the total volume of the system. After the aggregation of particles at the first critical field, it is natural that the chains will be distributed uniformly spanning the entire volume of the cell due to the homogeneity of field in the region of interest. Therefore, considering the hexagonal arrangement of the chains the position coordinate of the particles are found out. Similarly, following the same procedure at higher critical fields also the columns of various diameters are distributed uniformly, so that they span the entire volume. While finding the position coordinate of particles in a system consisting of columns with more than one chain, it is considered that the chains are hexagonally close packed to each other in each column [48]. Now, the position coordinates of the particles for different configurations (Fig. 4) both before and after aggregation at various critical fields are known. Therefore, using this information the total potential energy of the system for the different cases as discussed in Fig. 4 are calculated and compared.

Suppose that the total number of particles in the system is 200 and that they are dispersed in a box of volume $44a \times 34a \times 5a \text{ nm}^3$, where $a=1.35d$ and d is the diameter of each particle. Using [Eq. (8)] the IPS for the magnetic nanoparticles dispersion of a given particle volume fraction is calculated to be 46 nm. The energy of the system before aggregation at the first critical field is $1.22 \times 10^{-26} \text{ J}$. The total interaction energy for this system after aggregation at first critical field is calculated to be $-5.36 \times 10^{-25} \text{ J}$ and it increases to $-1.2 \times 10^{-24} \text{ J}$ before aggregation at the second critical field. After aggregation the total system energy decreases to $-1.05 \times 10^{-24} \text{ J}$ at the second critical field itself. The system energy increases to $-1.86 \times 10^{-24} \text{ J}$ at the third critical field. This energy gets decreased to $-1.42 \times 10^{-24} \text{ J}$ after aggregation at the third critical field which further increases to $-2.21 \times 10^{-24} \text{ J}$ before aggregation at the fourth critical field. The total energy again gets decreased after aggregation at the fourth critical to $-1.4 \times 10^{-24} \text{ J}$. Therefore, the energy gets decreased once they form columns at higher critical fields. This decrease in the total system energy strongly supports the argument that the chains undergo lateral aggregation at different critical fields. By undergoing this kind of lateral aggregation of the chains among themselves at different critical fields, the system goes to lower and lower-energy state, which is clear from the interaction energy calculation.

For two rigid chains of magnetic colloids aligned parallel to one another, the interaction energy curve consists of two parts: (1) an attractive energy well if the chains have a net attraction once they have zipped and (2) a repulsive interac-

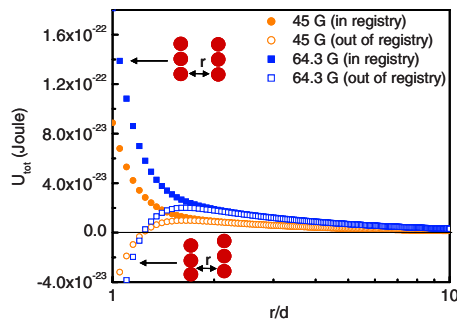


FIG. 5. (Color online) Interaction energy between two chains, each containing 50 magnetic particles, as a function of their spacing at the first and second critical fields when the chains are in and out of registry. The configuration of particles under the above two conditions are shown in the inset.

tion for parallel chains (of the same length) as they approach one another laterally [40,41]. When the chains are of different lengths or shifted with respect to one another (off registry), zippering of chains can take place due to attractive energy well. The lowest-energy state of the system as predicted by the Gross model consists of clusters containing zipped chains [41].

Haghighi and Doyle calculated the exact form of interaction energy for two rigid chains by simply summing the dipole-dipole interactions between all of the colloids in the two chains [40]. They demonstrate that head-to-tail aggregation is necessary to form the single chains and does not involve any significant energy barrier, and therefore the system is not kinetically limited from reaching the lowest-energy state. Their model for energy barrier incorporates the effects of volume fraction to account for additional net attraction forces between chains due to the surrounding chains.

Figure 5 shows the form of interaction energy between two chains each containing 50 magnetic particles as a function of their spacing for the first and second critical fields

when the chains are in and out of registry. The alignment of particles under the above two conditions are shown in the inset of Fig. 5. The magnitude of this energy barrier at the first critical field is $\sim 1.0 \times 10^{-23}$ J. At the second critical field when the magnetic field is increased by 20 G, this energy barrier gets increased to $\sim 2.0 \times 10^{-23}$ J. The difference of these two energies is 1.0×10^{-23} J that is the exact energy required for the lateral aggregation of the two chains. This balance energy is used to overcome the energy barrier for the lateral aggregation of the chains formed by the magnetic particles in the presence of external magnetic. This is one of the plausible reasons for the occurrence of zippering at every 20 G, above the first critical magnetic field. Since the system is continuously evolving under external magnetic field, it appears that the chains undergoes a coarsening with time.

IV. CONCLUSION

The transmitted intensity and the scattered pattern show time-dependent variation at different critical fields upon slow ramping of external field. Several critical fields are observed at a regular interval of 20 G after the first critical field. At each critical field, the transmitted light intensity decreases drastically followed by the formation of a ringlike pattern on a screen placed perpendicular to the field direction. The observed critical fields are attributed to zippering transitions of the chains due to attractive energy well when the chains are of different lengths or shifted with respect to one another. Calculations show a decrease in energy of the system due to dipolar interactions at different critical fields, confirming the coarsening of the field-induced structures that lower the system energy.

ACKNOWLEDGMENTS

The authors would like to thank Dr. P. R. Vasudeva Rao and Dr. T. Jayamumar for useful discussions.

-
- [1] A. Yethiraj and A. van Bladder, *Nature (London)* **421**, 513 (2003).
 [2] D. A. Weitz, J. S. Huang, M. Y. Lin, and J. Sung, *Phys. Rev. Lett.* **53**, 1657 (1984).
 [3] P. C. Hiemenz and R. Rajagopalan, *Principles of Colloid and Surface Chemistry* (Marcel Dekker, New York, 1997).
 [4] S. John, *Phys. Rev. Lett.* **53**, 2169 (1984).
 [5] P. E. Wolf and G. Maret, *Phys. Rev. Lett.* **55**, 2696 (1985).
 [6] D. S. Wiersma, P. Bartolini, A. Lagendijk, and R. Righini, *Nature (London)* **390**, 671 (1997).
 [7] J. Philip, G. Gnana Prakash, T. Jaykumar, P. Kalyanasundaram, and B. Raj, *Phys. Rev. Lett.* **89**, 268301 (2002).
 [8] J. J. Chieh, S. Y. Yang, H. E. Horng, C. Y. Hong, and H. C. Yang, *Appl. Phys. Lett.* **90**, 133505 (2007).
 [9] H. E. Horng, C. S. Chen, K. L. Fang, S. Y. Yang, J. J. Chieh, C. Y. Hong, and H. C. Yang, *Appl. Phys. Lett.* **85**, 5592 (2004).
 [10] A. F. Bakuzis, K. Skeff Neto, P. P. Gravina, L. C. Figueiredo, P. C. Morais, L. P. Silva, R. B. Azevedo, and O. Silva, *Appl. Phys. Lett.* **84**, 2355 (2004).
 [11] J. Philip, P. D. Shima, and B. Raj, *Appl. Phys. Lett.* **91**, 203108 (2007).
 [12] J. Liu, E. M. Lawrence, A. Wu, M. L. Ivey, G. A. Flores, K. Javier, J. Bibette, and J. Richard, *Phys. Rev. Lett.* **74**, 2828 (1995).
 [13] G. A. Flores, J. Liu, M. Mohebi, and N. Jamasbi, *Phys. Rev. E* **59**, 751 (1999).
 [14] M. Fermigier and A. P. Gast, *J. Colloid Interface Sci.* **154**, 522 (1992).
 [15] D. Wirtz and M. Fermigier, *Phys. Rev. Lett.* **72**, 2294 (1994).
 [16] E. M. Furst and A. P. Gast, *Phys. Rev. E* **62**, 6916 (2000).
 [17] A. J. Dickstein, S. Erramilli, R. E. Goldstein, D. P. Jackson, and S. A. Langer, *Science* **261**, 1012 (1993).
 [18] A. Hynninen and M. Dijkstra, *Phys. Rev. Lett.* **94**, 138303 (2005).
 [19] S. Melle, M. A. Rubio, and G. G. Fuller, *Phys. Rev. Lett.* **87**, 115501 (2001).

- [20] D. Heinrich, A. R. Goni, and C. Thomsen, *J. Chem. Phys.* **126**, 124701 (2007).
- [21] J. H. E. Promislow, A. P. Gast, and M. Fermigier, *J. Chem. Phys.* **102**, 5492 (1995).
- [22] F. Martínez-Pedredo, A. El-Harrak, J. C. Fernandez-Tolenado, M. Tirado-Miranda, J. Baudry, A. Schmitt, J. Bibette, and J. Callejas Fernandez, *Phys. Rev. E* **78**, 011403 (2008).
- [23] F. Martínez-Pedredo, M. Tirado Miranda, A. Schmitt, and J. Callejas Fernandez, *J. Chem. Phys.* **125**, 084706 (2006).
- [24] A. Wiedenmann, U. Keiderling, K. Habicht, M. Russina, and R. Gahler, *Phys. Rev. Lett.* **97**, 057202 (2006).
- [25] M. C. Miguel and R. Pasto-Satorras, *Phys. Rev. E* **59**, 826 (1999).
- [26] P. D. Duncan and P. J. Camp, *J. Chem. Phys.* **121**, 11322 (2004).
- [27] P. D. Duncan and P. J. Camp, *Phys. Rev. Lett.* **97**, 107202 (2006).
- [28] T. Ukai and T. Maekawa, *Phys. Rev. E* **69**, 032501 (2004).
- [29] M. Mohebi, N. Jamasbi, and J. Liu, *Phys. Rev. E* **54**, 5407 (1996).
- [30] C. Rablau, P. Vaishnava, C. Sudakar, R. Tackett, G. Lawes, and R. Naik, *Phys. Rev. E* **78**, 051502 (2008).
- [31] S. Cutillas and J. Liu, *Phys. Rev. E* **64**, 011506 (2001).
- [32] M. Ivey, J. Liu, Y. Zhu, and S. Cutillas, *Phys. Rev. E* **63**, 011403 (2000).
- [33] Y. H. Hwang and X.-L. Wu, *Phys. Rev. E* **49**, 3102 (1994).
- [34] M. F. Islam, K. H. Lin, D. Lacoste, T. C. Lubensky, and A. G. Yodh, *Phys. Rev. E* **67**, 021402 (2003).
- [35] B. Hoffmann and W. Kohler, *J. Magn. Magn. Mater.* **262**, 289 (2003).
- [36] M. F. da Silva and A. M. Figueiredo Neto, *Phys. Rev. E* **48**, 4483 (1993).
- [37] H. D. Deng, J. Liu, W. R. Zhao, W. Zhang, X. S. Lin, T. Sun, Q. F. Dai, L. J. Wu, S. Lan, and A. V. Gopal, *Appl. Phys. Lett.* **92**, 233103 (2008).
- [38] T. C. Halsey and W. Toor, *Phys. Rev. Lett.* **65**, 2820 (1990).
- [39] J. E. Martin, J. Odinek, and T. C. Halsey, *Phys. Rev. Lett.* **69**, 1524 (1992).
- [40] R. Haghgooeie and P. S. Doyle, *Phys. Rev. E* **75**, 061406 (2007).
- [41] M. Gross, *Phys. Rev. E* **58**, 6124 (1998).
- [42] J. E. Martin, K. M. Hill, and C. P. Tigges, *Phys. Rev. E* **59**, 5676 (1999).
- [43] J. Li, X. D. Liu, Y. Q. Lin, Y. Huang, and L. Bai, *Appl. Phys. B: Lasers Opt.* **82**, 81 (2006).
- [44] T. C. Halsey and W. Toor, *J. Stat. Phys.* **61**, 1257 (1990).
- [45] J. M. Laskar, J. Philip, and B. Raj, *Phys. Rev. E* **78**, 031404 (2008).
- [46] J. Philip, J. M. Laskar, and B. Raj, *Appl. Phys. Lett.* **92**, 221911 (2008).
- [47] T. Hao and R. E. Riman, *J. Colloid Interface Sci.* **297**, 374 (2006).
- [48] M. Klokkenburg, B. H. Erne, J. D. Meeldijk, A. Wiedenmann, A. V. Petokov, R. P. A. Dullens, and A. P. Philipse, *Phys. Rev. Lett.* **97**, 185702 (2006).